Available online at www.sciencedirect.com
ScienceDirect
Computer Aided Geometric Design 26 (2009) 105–116
COMPUTER AIDED GEOMETRIC DESIGN
www.elsevier.com/locate/cagd

Guided spline surfaces

K. Karčiauskas [a], J. Peters [b,*]

[a] *Department of Mathematics and Informatics, Naugarduko 24, 03225 Vilnius, Lithuania*
[b] *University of Florida, Department of CISE, CSE Building 32611-6120, Gainesville, FL, United States*

Received 9 January 2007; received in revised form 27 November 2007; accepted 3 December 2007

Available online 15 December 2007

Abstract

We separate the conceptual design and the representation of high quality surfaces by prescribing local shape via guide surfaces and then sampling these guides with a finite number of tensor-product patches. The paper develops a *family of algorithms* that allow trading polynomial degree for smoothness near the extraordinary points where more or fewer than four tensor-product patches meet. A key contribution are rules for a *capping of a multi-sided hole by a small number of polynomial patches*. The construction of highest quality creates first a G^1 cap of patches of degree $(6, 6)$ and then perturbs it to yield an exact G^2 cap of degree $(8, 8)$. Since this perturbation is so small that its effect is typically not perceptible even in curvature display, the unperturbed surface of degree $(6, 6)$ is an excellent alternative. Reducing the degree of the rings to $(5, 5)$, respectively $(4, 4)$, by choice of a different parameterization, increases the number of G^1 transition curves within the cap but does not alter the shape appreciably.

1. Introduction

Constructing a multi-sided piecewise polynomial surface piece to complete a C^2 tensor-product surface where n pairwise-joined primary surfaces join is a key task of geometric design. The challenge is to complete the surface without introducing curvature artifacts such as discontinuities or oscillations. Our approach here is novel in that the multi-sided piecewise polynomial surface piece is constructed following a guiding surface that encodes the design intent by its shape. The advantage of such guided constructions is the regional, larger-scale determination of shape that avoids the oscillations of purely local constructions. In particular, simple local averaging rules, as used in subdivision constructions, e.g. (Catmull and Clark, 1978), often introduce artifacts in the first steps (Augsdörfer et al., 2006).

The guide surface itself can typically not be used directly to complete the surface, because it does not fit functional requirements (it may not even join the existing surface complex continuously—see e.g. Fig. 1 of Karčiauskas and Peters, 2007a) or the requirements of a geometry processing pipeline (because it is of high degree or non-polynomial). The approach taken in this paper builds on the construction of guided surface rings (Karčiauskas and Peters, 2007a). There, in the spirit of subdivision algorithms, a sequence of nested surface rings $\mathbf{x}^m$ is constructed that fills an n-sided hole in a C^2 spline complex (Fig. 1, *left*) so that the surface resulting from the *infinite* sequence is C^2 and piecewise polynomial of degree $(6, 6)$. We review this construction in Section 2. Here, we replace the infinite sequence by

* Corresponding author.
E-mail addresses: kestutis.karciauskas@mif.vu.lt (K. Karčiauskas), jorg@cise.ufl.edu (J. Peters).

0167-8396/$ – see front matter
doi:10.1016/j.cagd.2007.12.002

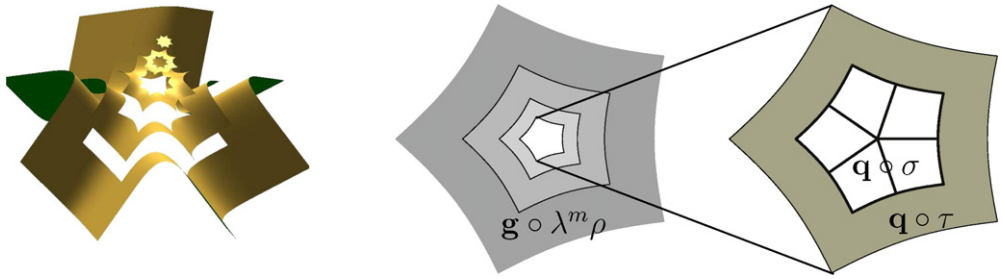

Fig. 1. (*left*) Sequence of guided surface rings and cap in $\mathbb{R}^3$, offset to show the structure. (*middle* and *right*) Structure of the finite construction. (*middle*) Surface rings $\mathbf{x}^m := H(\mathbf{g} \circ \lambda^m \rho)$ of degree (d, d) constructed according to Karčiauskas and Peters (2007a). Here $d = 6$ leads to the construction of highest quality; $d = 4$ is the lowest degree considered in this paper. (*right*) The focus of this paper: the transition pieces $H(\mathbf{q} \circ \tau)$ of degree (d, d) and the n Bézier patches of degree (d^*, d^*), derived from $\mathbf{q} \circ \sigma$, forming the final cap. (Rotated copies of σ and τ together form the map $\mu : [0..1]^2 \times \{1, \ldots, n\} \to \mathbb{R}^2$.) Here $d^* = 8$ for highest quality; but $d^* = 4$ allows for an approximation of only slightly lower quality (see Fig. 14).

no more than three rings plus a final capping patchwork consisting of tensor-product patches. This final capping patchwork is the focus of the paper and is explained in Section 4. Formally, the initial three guided rings are not needed to apply the constructions of this paper. However, our experience with these constructions over the last years shows that such intermediate rings improve the curvature distribution and final shape. Since kth order terms decay by λ^k with each ring (where $\lambda < 1$ is the subdominant eigenvalue of Catmull–Clark subdivision), we can replace the initial higher-degree guide $\mathbf{g}$ after three steps by a C^2 piecewise polynomial guide $\mathbf{q}$ of total degree 4 (and in certain cases degree 3) rather than the guide $\mathbf{g}$ of degree 5 or higher used to construct the initial rings that have to match generic boundary data.

The main remaining task is to choose a good *parametrization (tessellation) of the domain* of $\mathbf{q}$, namely a *finite tessellation map* μ that maps the domains of the individual sectors to form a neighborhood of the origin the domain of $\mathbf{q}$ (cf. Fig. 1 and Section 3). Given $\mathbf{q}$ and μ, the surface construction in Section 4 consists of two simple steps: applying an operator H defined in Section 2 and perturbing three coefficients. Section 4.1 shows the remarkable fact that leaving out this final perturbation yields visually unchanged, high-quality surfaces of degree $(6, 6)$. Section 5 develops two constructions of still lower-degree, illustrating the flexibility gained by separating issues of shape and final surface representation.

2. Review of literature and basic tools

2.1. Some curvature continuous surface constructions

Despite many improvements, classical subdivision algorithms acting on a *local control net* have to date not reached the quality needed for A-class design. The only C^2 constructions, Karčiauskas and Peters (2007a) and Karčiauskas et al. (2006), inherit their good curvature distribution from non-local guides. The publications (Gregory and Hahn, 1989; Prautzsch, 1997; Reif, 1998; Peters, 2002a) represent some well-known algorithms for generating C^2 (curvature continuous) surfaces consisting of a *finite number* of tensor-product spline pieces that can be arranged in an unrestricted patch layout. For these approaches, shape problems are known to occur in the transition between the regular regions that make up the bulk of the surface and the immediate neighborhood of *extraordinary points* where $n \neq 4$ surface pieces meet. Moreover, algorithms like (Loop, 2004), that could be adjusted to improve the transition, base their relatively low degree on the assumption that the boundary data are bicubic. Bicubics, however, are too restrictive for fair design in general. For example, blends between cylinders naturally lead to boundary data of degree 5 or 6. Alternative non-polynomial schemes include high-degree rational representations (Grimm and Hughes, 1995; Cotrina Navau and Pla Garcia, 2000; Karciauskas and Peters, 2004) and representations based on exponential functions and roots of polynomials (Ying and Zorin, 2004; Levin, 2006). A number of these schemes assume that the input control net is generated by two or more Catmull–Clark refinement steps. Such preprocessing is likely to introduce shape problems due to the dominance of the hyperbolic terms in Catmull–Clark subdivision (Karciauskas et al., 2004). Imposing regional control via a guide surface was already used in Prautzsch (1997), Reif (1998). There, the main motivation for using guide surfaces was to ensure C^2 continuity; by contrast, here we emphasize the use of the

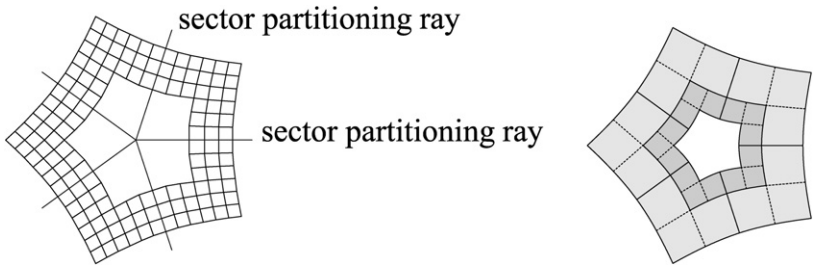

Fig. 2. ct-map. (*left*) Bézier coefficients of one (bicubic) ring of a ct-map with □-sprocket (Catmull–Clark) layout. The sectors are bounded by rays. (*right*) Two nested ct-maps.

guide for regional shape control. Since the surfaces in Prautzsch (1997), Reif (1998) are of degree $(3d, 3d)$, where d is the degree of the guide, $d \leqslant 3$ was chosen to keep the degree of the final surface manageable. However, guides of degree $d \leqslant 3$ result in general in undesirable transitions from the regular surface region to the extraordinary point, especially for higher-order saddles. Entire polynomials were also chosen in Ying and Zorin (2004) and Levin (2006), but there the degree of the guide does not play a role since neither scheme generates polynomial or rational surfaces. Restricting the guides to be entire polynomials makes the resulting surfaces less expressive and flexible than using piecewise polynomial guides (Peters, 2002a).

2.2. Guided surface rings

Given a local guide, a nested sequence of surface rings can be generated by a general procedure. The tensor-product-spline compatible surface rings defined in Karčiauskas and Peters (2007a) consist of quadrilateral patches arranged like a sprocket and therefore called □-*sprocket rings*. Each ring consists of $3n$ patches of degree $(6, 6)$ that join to yield a C^2 surface with the structure of Fig. 2, *right*. The first sprocket ring can match second-order spline data at its outer n consecutive boundary curves, for example join C^2 with a bicubic spline complex, or degree (k, k) spline complex, $k < 7$. (Such higher degree boundary data occur naturally when blending quadrics.) The surface rings $\mathbf{x}^m$ are constructed by *sampling* the composition $\mathbf{g} \circ \lambda^m \rho$, where $\mathbf{g}: \mathbb{R}^2 \to \mathbb{R}^3$ is the guide and ρ a concentric tessellation map, *ct-map* for short, i.e. a map whose scaled images $\lambda^m \rho$, $m = 0, 1, \ldots$ tessellate the neighborhood of the origin by a sequence of nested, concentric annuli (see Fig. 2, *right*). Here, we will construct only a few (at most 3) annuli and complete the neighborhood of the origin by a finite tessellation (map) σ connected to ρ via a transition tessellation annulus τ.

2.3. Hermite sampling

Here, and in the following, we assume that the reader is familiar with the Bézier representation of polynomials and their derivatives along boundaries in terms of 'layers of coefficients', as well as the concept of 'degree-raising' and geometric continuity as explained in the standard textbooks (Farin, 1988; Prautzsch et al., 2002) and the Handbook of Computer Aided Geometric Design (see e.g. Peters, 2002b). A central component of the construction in Karčiauskas and Peters (2007a) is the *Hermite sampling* operator h that is ultimately modified to an operator H that guarantees that rings join C^2. When applied to a map $f(s, t)$ defined over unit square, $h^{6,6}$ creates a patch of degree $(6, 6)$ as follows.

- At each corner, the partial derivatives of $f(s, t)$

$$\begin{array}{cccc} \partial_t^3 f & \partial_s \partial_t^3 f & \partial_s^2 \partial_t^3 f & \partial_s^3 \partial_t^3 f \\ \partial_t^2 f & \partial_s \partial_t^2 f & \partial_s^2 \partial_t^2 f & \partial_s^3 \partial_t^2 f \\ \partial_t f & \partial_s \partial_t f & \partial_s^2 \partial_t f & \partial_s^3 \partial_t f \\ f & \partial_s f & \partial_s^2 f & \partial_s^3 f \end{array}$$

  are sampled and converted into 4×4 corner block of Bézier coefficients of a polynomial piece of degree $(6, 6)$ (Fig. 3, *left*).
- At overlapping positions, the coefficients are averaged (Fig. 3, *left right*).

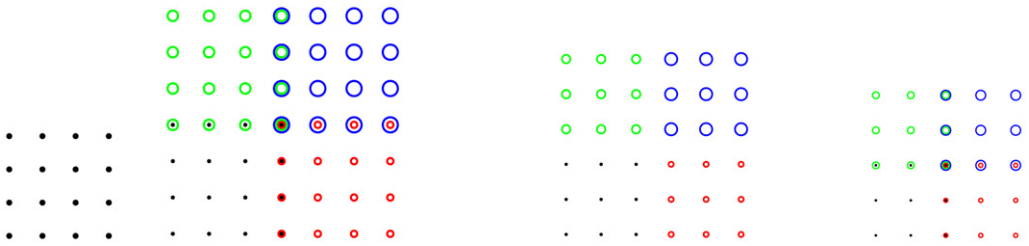

Fig. 3. (*left*) Sampled 4×4 corner block in Bézier form; four such blocks are overlapped to form a patch of degree $(6, 6)$. (*middle*) The same construction combines four 3×3 blocks into a patch of degree $(5, 5)$ or (*right*) of degree $(4, 4)$.

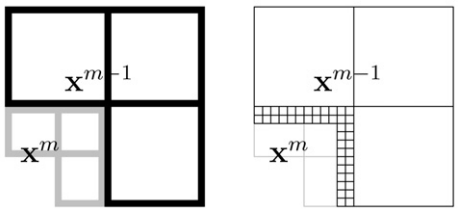

Fig. 4. (*left*) Structure of the sampled patches of degree $(6, 6)$ of two consecutive rings in one sector (cf. Fig. 2). (*right*) Joining the patches C^2 by (inward) prolongation: the three corresponding layers of propagated Bézier coefficients are shown as a fine grid.

Fig. 3, *middle* and *right* illustrate two similar sampling constructions that generate maps of lower bi-degree. Hermite sampling will in the following be applied to the composition of a C^2 guide $\mathbf{g}$ with one of the planar tessellation maps σ, τ or ρ defined below. The degree of the guide can, for example, be as high as total degree 14 and it is composed with a tessellation map that can be of degree $(5, 5)$. The Hermite sampling process decouples such high degree from the degree of the resulting surface rings.

To insure that the sampled patches of degree (d, d) will join C^2, respectively G^2 when $h^{d,d}$ is applied to each piece of $\mathbf{g} \circ \mu$, we align the *sector partitioning rays* of μ (Fig. 2) with the domain boundaries of the pieces of $\mathbf{g}$.

2.4. Prolongation

The operator H adjusts the preliminary rings created by $h^{d,d}$ so that the coarser ring $\mathbf{x}^{m-1}$ defines the outer boundary derivatives of the inserted finer ring $\mathbf{x}^m$ at the transition. That is, the innermost layers of the outer ring $\mathbf{x}^{m-1}$ (with the coarser patch layout) determine the three outermost layers of Bézier coefficients of the inner ring $\mathbf{x}^m$ (Fig. 4).

3. The finite tessellation map μ mapping to the domain of the guide q

We will construct the surface cap as a perturbation of $H(\mathbf{q} \circ \mu)$, where $\mathbf{q} : \mathbb{R}^2 \to \mathbb{R}^3$ is a guide surface. The bivariate planar, piecewise polynomial, finite tessellation

$$\mu : [0..2]^2 \times \{1, \ldots, n\} \to \mathbb{R}^2,$$

maps to an n-sided disk and consists of n segments, each a rotation by R^k, $k \in \{1, \ldots, n\}$ of a single sector prototype map

$$\sigma \cup \tau, \quad \text{where } R \text{ the matrix of rotation by } 2\pi/n.$$

The prototype map itself consists of four pieces, each of degree $(5, 5)$: the central piece σ at the origin and the surrounding transition map τ consisting of three pieces (see Fig. 5). The n rotated copies tessellate a neighborhood of the origin.

The transition map τ is constructed to be

- internally C^2,
- join C^2 with its rotated neighbors, $R\tau$ and $R^{-1}\tau$,

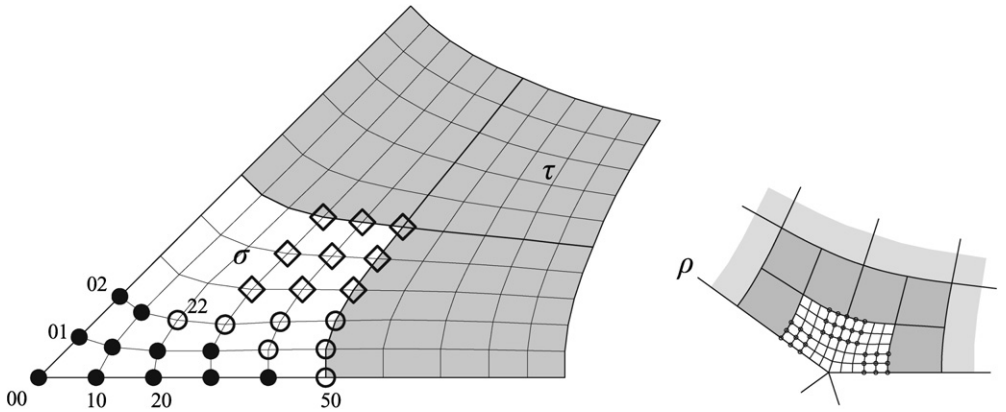

Fig. 5. (*left*) The Bézier net of one sector of μ for $n = 8$. The sector is defined by four maps each of degree $(5, 5)$ and mapping from the unit square to $\mathbb{R}^2$. The origin coincides with the Bézier coefficient labeled 00. The map σ (no gray underlay) is constructed to have low degree across the sector partitioning rays. Scalar degrees of freedom in the construction of σ are indicated as *circles* and *diamonds*. (*right*) The maps σ and $R\sigma$ join C^2 at the corner points $(s, t) \in \{(0, 1), (1, 0)\}$ by choice of the coefficients indicated as $\circ$.

– join C^2 with the innermost prolongation of the ct-map ρ, and
– join C^2 with σ.

Since τ is piecewise of degree $(5, 5)$, this implies the following lemma (see gray area in Fig. 5).

Lemma 1. *The map τ is determined by the C^2 constraints with ρ and σ.*

Lemma 1 allows us to focus exclusively on the construction of σ (see Fig. 5). The map

$$\sigma : [0..1]^2 \to \mathbb{R}^2,$$
$$(s, t) \mapsto \sum_{i=0}^{5} \sum_{j=0}^{5} \sigma_{ij} b_i(s) b_j(t), \quad b_i(s) := \binom{5}{i} (1-s)^{5-i} s^i,$$

is constructed so that (cf. Fig. 5)

– σ and $R\sigma$ join C^2 at the corners $(s, t) \in \{(0, 1), (1, 0)\}$,
– σ is symmetric with respect to its bisectrix, $s = t$,
– σ and $R\sigma$ are symmetric with respect to the sector partitioning ray, and
– the ith derivative of σ across the boundary $t = 0$, evaluated along the edge $t = 0$, is of degree $2i + 1$ for $i = 0, 1, 2$ (see Lemma 2).

That is, the reflection across the bisectrix maps σ_{ij} into σ_{ji}, the boundaries are parametrized as straight lines of degree 1 and the first derivative across each sector boundary is of degree 3. The symmetry with respect to the sector partitioning ray is implied by bisectrix-symmetry and rotation. The *sector edges* are $\mathbf{0}\mathbf{v}_0$ and $\mathbf{0}\mathbf{v}_1$ where $\mathbf{0} := (0, 0)$, $\mathbf{v}_0 := \kappa_0(1, 0)$ (κ_0 a free parameter) and $\mathbf{v}_1 := R\mathbf{v}_0$. The Bézier coefficients of σ are then determined as follows (cf. Fig. 6).

(i) $\sigma(s, 0)$ is linear: $\sigma_{i0} := (1 - i/5)\mathbf{0} + (i/5)\mathbf{v}_0$, $i = 0, \ldots, 5$; the points σ_{0i} are symmetric to the points σ_{i0}, i.e. $\sigma_{0i} := (1 - i/5)\mathbf{0} + (i/5)\mathbf{v}_1$, $i = 0, \ldots, 5$.
(ii) $\partial_t \sigma(s, 0)$ is cubic, i.e. σ_{i1}, $i = 0, \ldots, 5$, define a cubic in degree-raised form. Due to symmetry across the sector partitioning ray and C^1 continuity at $\mathbf{v}_0$, the line segments σ_{i1}, σ_{i0}, $i = 3, 4, 5$, must be perpendicular to the edge $\sigma(s, 0)$ and, by symmetry, σ_{11} must be on the bisectrix between $\sigma(s, 0)$ and $\sigma(0, t)$. Since σ_{01} is fixed by (i), these four additional constraints on the 8 degrees of freedom of the cubic leave one degree of freedom each for the points σ_{41} and σ_{51}.

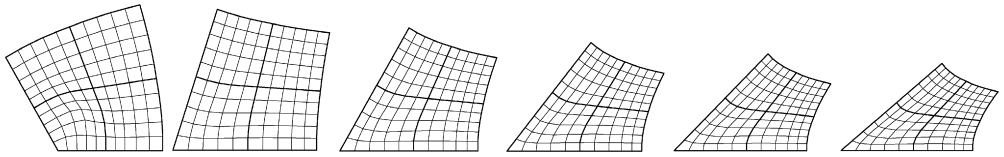

Fig. 6. Sector of the map μ for $n = 3, 5, 6, 7, 8, 9$ (for $n = 4$, the map is the identity).

(iii) By symmetry, σ_{22} is on the bisectrix; by C^2 continuity at $\mathbf{v}_0$, the distances of the points σ_{i2}, $i = 3, 4, 5$, to the edge $\mathbf{0}$, $\mathbf{v}_k$ must be twice those of σ_{i1}.

Since the remaining points σ_{ij}, $3 \leqslant i, j \leqslant 5$ (*diamond*-shaped points in Fig. 5) are free except for symmetry, the map σ has $7 + 9 = 16$ free scalar parameters.

Denote by

$$\deg_E(f)$$

the degree of a map f restricted to the *sector edge* (line segment) $E := ([0, 1], 0)$ that σ maps to the straight line parametrized by the coefficients with the indices $00, 10, \ldots, 50$. Then, regardless of the choice of the remaining parameters, the following holds by construction.

Lemma 2. *For* $\alpha \in \{0, 1, 2\}$, $\deg_E(\partial_t^\alpha \sigma) = 2\alpha + 1$.

The free parameters are optimized in two steps. First, all free parameters except σ_{22} (*circle* in Fig. 5) are determined by minimizing $\mathcal{F}_5(\tau^1) + \mathcal{F}_5(\tau^2) + \mathcal{F}_5(\tau^3)$ where τ^i are the three pieces of τ and $\mathcal{F}_k(f_1, f_2) := \mathcal{F}_k(f_1) + \mathcal{F}_k(f_2)$ and

$$\mathcal{F}_k(f) := \int_0^1 \int_0^1 \sum_{i+j=k, i,j \geqslant 0} \binom{k}{i} \left(\partial_s^i f \partial_t^j f\right)^2. \tag{1}$$

Then σ_{22} is determined by minimizing the functional $\mathcal{F}_5(\sigma)$. Note that the functional is applied only to the planar map μ and not to the surface $\mathbf{q} \circ \mu$. Moreover, this optimization, as well as (i), (ii), (iii) above, are independent of the geometry. Therefore the tessellation needs to be computed only once ever and then tabulated or coded as a subroutine in n. Fig. 6 shows one sector of μ up to $n = 9$.

4. The surface cap in $\mathbb{R}^3$

The operator H (see Section 2.4) decouples the degree of the composition of guide and tessellation map from the degree of the resulting surface ring. However, for the cap, we need a low-degree guide to arrive at a final surface that has low degree. After three guided surface rings, piecewise quartic guides do well since, in the mth ring, the kth order terms have decayed to λ^{-km} their original size where $\lambda < 1$ is the subdominant eigenvalue of Catmull–Clark subdivision. So we may replace the initial guide $\mathbf{g}$ (Section 2.2) by a C^2 piecewise polynomial guide $\mathbf{q}$ of total degree $d = 4$. Choosing $d = 5$ yields an analogous algorithm that preserves shape well using only one instead of three rings guided by $\mathbf{g}$ before switching to $\mathbf{q}$. Formally, for the continuity of the surface (as expressed in Theorem 1, below), we need not generate any of the three rings; however, we recommend the rings as a preparation to obtain highest-quality curvature distribution over the cap. In either case, boundary data up to degree $(6, *)$, i.e. up to degree 6 along the boundary, can be matched by the construction. In our setting, the boundary data are represented as three layers of Bézier coefficients prolongated from a guided ring of degree $(6, 6)$.

Given μ defined in Section 3, the algorithm is very simple.

(a) For $k = 1, \ldots, n$, compute a preliminary cap consisting of the $4n$ pieces $H(\mathbf{q} \circ R^k \sigma)$ and $H(\mathbf{q} \circ R^k \tau)$ of degree $(6, 6)$ (Fig. 7, *middle*);
Join the cap C^2 to the surrounding guided surface ring by prolongation.

(b) For $k = 1, \ldots, n$, degree-raise $H(\mathbf{q} \circ R^k \sigma)$ to $(8, 8)$ and replace the coefficients circled in Fig. 7, *right*, by the corresponding coefficients of the $\alpha = 2$ boundary layer of $\mathbf{q} \circ R^k \sigma$ represented as a polynomial of degree 8.

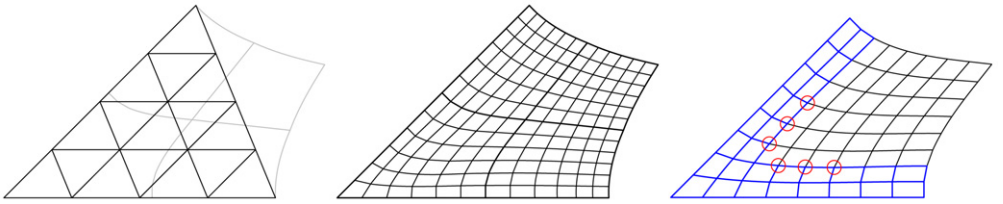

Fig. 7. (*left*) Layout of the four range quadrilaterals of σ and τ with the triangulated domain of $\mathbf{q}$ superimposed. (*middle*) One sector of the preliminary cap consisting of four pieces of degree $(6,6)$. (*right*) Correction of innermost patches to obtain curvature continuity. Circled coefficients are from $\mathbf{q}\circ R^k\sigma$, all others from $H(\mathbf{q}\circ R^k\sigma)$, degree-raised to $(8,8)$.

(Lemma 3 below shows that the $\alpha=2$ boundary layer of $\mathbf{q}\circ R^k\sigma$ can be represented as a polynomial of degree 8 even though $\mathbf{q}\circ R^k\sigma$ is of degree $(20,20)$.)

The key observation focuses on the degree of the expansion of the composition $\mathbf{q}\circ\sigma$ when the geometry map $\mathbf{q}$ is of *total* degree d. Formally, the degree is $(5d,5d)$. However, by construction, along the sector partitioning rays, the degree is reduced to 1 and that of the first derivative to 3.

Lemma 3. *If* $d:=\deg(\mathbf{q})$ *then for* $\alpha\in\{0,1,2\}$, $\deg_E(\partial_t^\alpha\mathbf{q}\circ\sigma)=d+2\alpha$.

Proof. By Lemma 2, $\deg_E(\partial_t^\alpha\sigma)=2\alpha+1$. Then

$$\begin{aligned}
&\deg_E(\mathbf{q}\circ\sigma)=\deg_E\mathbf{q}=d,\\
&\deg_E\big(\partial_t(\mathbf{q}\circ\sigma)\big)=\deg_E(\partial\mathbf{q})\deg_E\sigma+\deg_E(\partial_t\sigma)=d-1+3,\\
&\deg_E\big(\partial_t^2(\mathbf{q}\circ\sigma)\big)=\max\big\{\deg_E(\partial^2\mathbf{q})\deg_E\sigma+2\deg_E(\partial_t\sigma),\deg_E(\partial\mathbf{q})\deg_E\sigma+\deg_E(\partial_t^2\sigma)\big\}\\
&\qquad\qquad=\max\{d-2+3+3,d-1+5\}=d+4.\qquad\square
\end{aligned}$$

Recall that the *sector edges* are the domain edges corresponding to the transition between the innermost patches $H(\mathbf{q}\circ R^k\sigma)$ and $H(\mathbf{q}\circ R^{k+1}\sigma)$.

Theorem 1. *The surface of degree* $(6,6)$ *created in step* (a) *is everywhere curvature continuous except that it is only tangent continuous across sector edges. After the perturbation* (b)*, the surface is everywhere curvature continuous.*

Proof. By construction with the operator H, the patches are of degree $(6,6)$ and join C^2 except across sector edges. By prolongation, the patches join C^2 with the surrounding ring of degree $(6,6)$. As the composition of a regular C^2 with a regular G^2 map, $\mathbf{q}\circ\mu$ is G^2. By Lemma 3, $H(\mathbf{q}\circ R^k\sigma)$ interpolates derivatives of sufficient degree to reproduce $\mathbf{q}\circ R^k\sigma$ up to first order along the sector edges. By construction with the operator H, both have the same second-order expansion at each endpoint of the edges. Therefore, the patchwork after step (a) is already G^1 along the central edges and curvature continuous at the extraordinary point. The perturbation (b) adjusts the second order continuity across sector edges to that of $\mathbf{q}\circ\mu$. Off hand $\mathbf{q}\circ\mu$ is of degree $(20,20)$. But only the boundary layers, defining the derivatives up to second order, are relevant for G^2 continuity and these are of lower degree. In particular, the second order transversal derivative along the boundary is only of degree $8=d+2\alpha=4+2\cdot 2$ for both maps and so perturbation (b) reproduces the G^2 joins in $\mathbf{q}\circ\mu$. $\square$

Fig. 8 illustrates the quality of the resulting surfaces.

4.1. A variant of degree $(6,6)$

Gauss curvature shaded images of surfaces with and without the perturbation step (b) above look identical, indicating that the perturbation, while technically necessary, is practically extremely small. That is, leaving out step (b), we obtain an almost curvature continuous cap of degree $(6,6)$. To analyze this phenomenon in more detail, we first

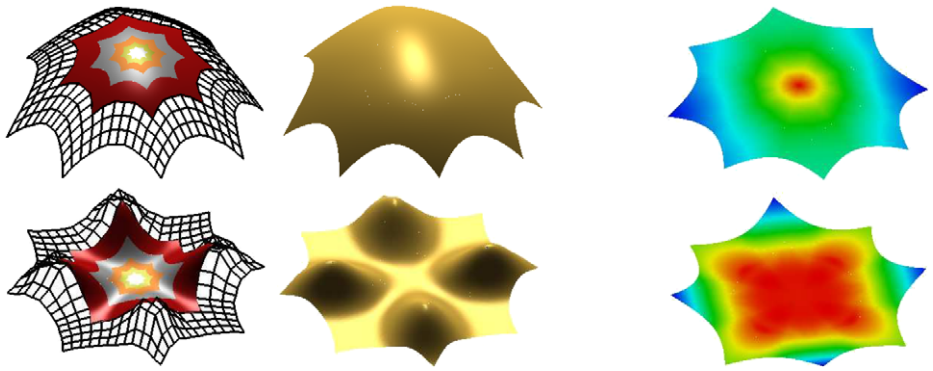

Fig. 8. C^2 surfaces of degree $(8,8)$. (*top*) Convex cap for convex data. (*bottom*) Multi-saddle. From *left* to *right*: (*left*) boundary data (shown as Bézier net), guided surface rings $H(\mathbf{g}\circ\rho)$ and $H(\mathbf{q}\circ\mu)$ and final cap; (*middle*) complete surface; (*right*) Gauss curvature shading of the last two rings and the cap.

observe that, if we had chosen $\mathbf{q}$ to be of degree $d=2$ then, by Lemma 3, the unperturbed construction would already be curvature continuous. Next, denote by w any scalar weight of a coefficient of $\mathbf{q}$ in the composition $\mathbf{q}\circ\mu$ of the exact C^2 join and by w^6 the corresponding weight in $H(\mathbf{q}\circ\mu)$, i.e. without the perturbation. Then for $n=8$, $(w-w^6)/w\leqslant .005$, i.e. the *maximum relative* change of weights is at most half a percent. It is therefore not surprising that this perturbation is not visible, even in the Gauss curvature display. For most applications, the simple construction of degree $(6,6)$ should therefore suffice.

5. G^1 caps of lower degree

By applying operators $h^{5,5}$, respectively $h^{4,4}$ to sample $\partial_s^i\partial_t^j(\mathbf{q}\circ\mu)$ for $i,j\in\{0,1,2\}$, we can still obtain C^2 guided surface rings, but the cap is now less smooth. Fig. 13, *middle*, juxtaposes the curves of curvature discontinuity of the three constructions.

5.1. A G^1 construction of degree $(5,5)$

Reducing the degree to the Hermite sampling operator to $(5,5)$, i.e. applying the operator $h^{5,5}$ (Fig. 3, *middle*), no longer guarantees G^1 continuity across sector partitioning rays, since, by Lemma 3, the first derivative of the composition of the guide of degree 4 and the reparametrization μ of degree $(5,5)$ is no longer reproduced along the sector partitioning ray. To guarantee G^1 continuity and retain as much as possible of the C^2 transitions of the construction of degree $(8,8)$, we choose σ of degree $(4,4)$ and so that

(i) σ is linear along the sector partitioning ray and
(ii) the first derivative of σ across the sector partitioning ray is of degree 2.

We choose the three pieces of τ to be of degree $(4,4)$ and construct them so that

(iii) τ and σ are C^1 connected everywhere and
(iv) τ and σ are C^2 connected along the sector partitioning ray.
(v) τ is C^2 and joins $R\tau$ in a C^2 fashion,
(vi) τ and ρ join C^2.

Fig. 9 shows the overall structure and the key parameters of the construction.

The construction of σ satisfying (i) through (v) leaves one degree of freedom for each *red circled*[1] point in Fig. 9, *left*. Specifically,

[1] For colors see the web version of this article.

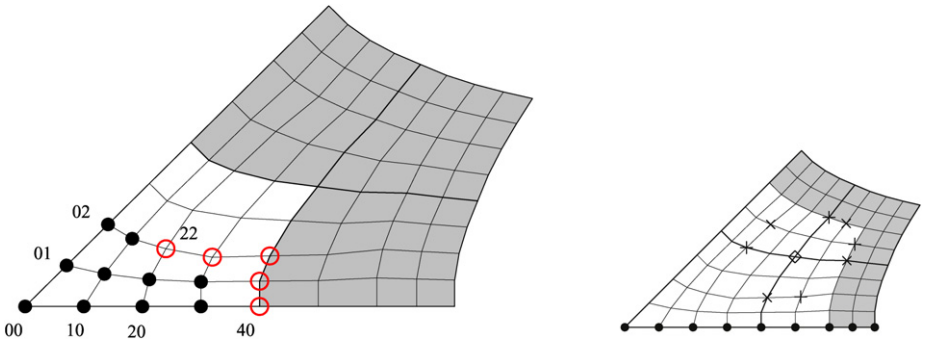

Fig. 9. (*left*) The Bézier net for $n = 8$ of one sector consisting of σ and the three pieces τ^1, τ^2 and τ^3 of τ (cf. Fig. 5). All maps are of degree $(4, 4)$. Scalar degrees of freedom in the construction of σ are indicated as *circles*. (*right*) Here gray indicates the subnet defined by C^2 prolongation of the regular, outer tessellation ρ. Nodes marked '$+$' and '$\times$' enter into a joint constraint. The central node marked $\diamond$ represents one scalar degree of freedom.

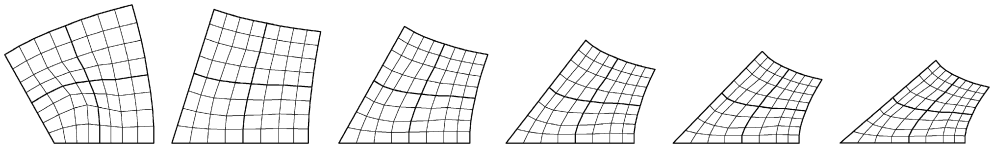

Fig. 10. The Bézier net of one sector consisting of the maps σ, τ^1, τ^2 and τ^3 of degree $(4, 4)$ for valence $n = 3, 5, 6, 7, 8, 9$.

(i′) σ_{s0} is linear: $\sigma_{i0} := (1 - i/4)\mathbf{0} + (i/4)\mathbf{v}_0$, $i = 0 \ldots 4$; the points σ_{0i} are symmetric to the points σ_{i0}.

(ii′) $\partial_t \sigma(s, 0)$ is quadratic, i.e. σ_{i1}, $i = 0 \ldots 4$, define a quadratic in degree-raised form. The segments σ_{i1}, σ_{i0}, $i = 3, 4$, must be perpendicular to the edge $\mathbf{0}$, $\mathbf{v}_0$ and, by symmetry, σ_{11} must be on the bisectrix between $\sigma(s, 0)$ and $\sigma(0, t)$.

(iii′, iv′) σ and τ are C^2 connected along the sector partitioning ray. Therefore, the distances of the points σ_{i2}, $i = 3, 4$, to the edge $\mathbf{0}$, $\mathbf{v}_0$ must be twice those of σ_{i1}, and σ_{40} is fixed.

(v′) The C^2 continuity of τ imposes the single constraint (cf. Fig. 9, *right*)

$$\sum\{\text{points marked as } +\} - \sum\{\text{points marked as } \times\} = 0.$$

(vi′) Three outer layers of Bézier coefficients are inherited from ρ.

The four remaining scalar parameters are (σ_{32} is determined by (v))

(a) the position of σ_{44} (*diamond*-shaped point) on the bisectrix in Fig. 9, *right*;
(b) the position of σ_{22} on the bisectrix;
(c) the distance of σ_{41} to the sector partitioning ray;
(d) the position of σ_{42} (its distance to the sector partitioning ray is twice that of σ_{41}).

These parameters are fixed by minimizing $\mathcal{F}_4(\tau^1) + \mathcal{F}_4(\tau^2) + \mathcal{F}_4(\tau^3) + \mathcal{F}_4(\sigma)$. The resulting tessellations are shown in Fig. 10.

Application of $h^{5,5}$ to the composition of this new tessellation map with $\mathbf{q}$ and C^2 prolongation inwards, yields patches of degree $(5, 5)$ with the following properties (cf. Fig. 13, *middle*).

Lemma 4. *The surface of degree* $(5, 5)$ *just constructed is everywhere curvature continuous except across the edges of* σ *where it is tangent continuous. The surface is curvature continuous at the extraordinary point.*

5.2. A G^1 construction of degree $(4, 4)$

A sequence of C^2 connected rings of degree $(4, 4)$ can, for example, be generated by converting sampled second order data from Bézier into B-spline form and averaging B-spline coefficients that overlap. Then, we can use the

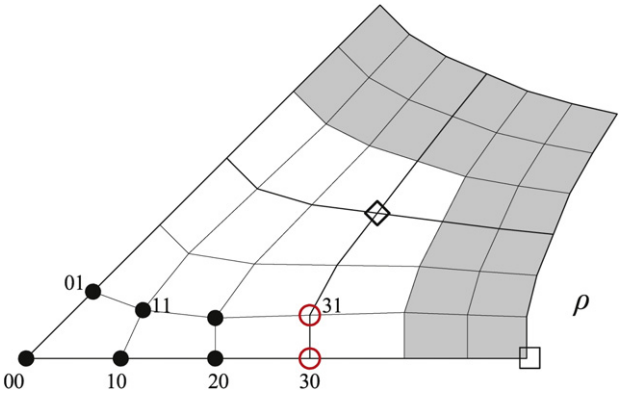

Fig. 11. Structure of σ and τ of degree $(3,3)$. Gray underlay indicates prolongation from ρ.

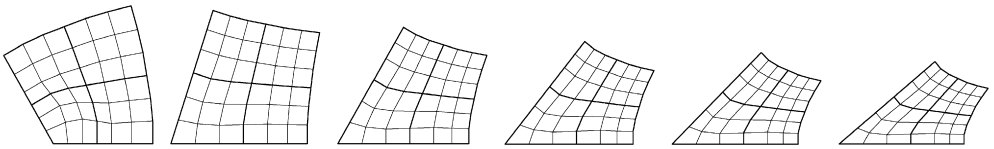

Fig. 12. The Bézier net of one sector consisting of the maps σ, τ^1, τ^2 and τ^3 of degree $(3,3)$ for valence $n = 3, 5, 6, 7, 8, 9$.

Hermite sampling operator $h^{4,4}$ of Fig. 3, *right* (that generates C^1 surfaces) to construct the cap. We choose σ of degree $(3,3)$ and, as in the previous two constructions, so that

(i) σ is linear along the sector partitioning ray, i.e. $\sigma_{i0} := (1 - i/3)\mathbf{0} + (i/3)\mathbf{v}_0$, $i = 0 \ldots 3$; the points σ_{0i} are symmetric to the points σ_{i0}.
(ii) the first derivative of σ across the sector partitioning ray is of degree 2, i.e. σ_{i1}, $i = 0 \ldots 3$, define a quadratic in degree-raised form. The segments σ_{i1}, σ_{i0}, $i = 2, 3$, must be perpendicular to the edge $\mathbf{0}, \mathbf{v}_0$ and, by symmetry, σ_{11} must be on the bisectrix between $\sigma(s, 0)$ and $\sigma(0, t)$.

This leaves two degrees of freedom (one for each *red* circled point).

We choose the three pieces τ^1, τ^2, τ^3 of τ of degree $(3,3)$ and so that (see Fig. 11)

(iii) τ and ρ join C^2 and
(iv) τ and σ are C^1 connected everywhere (this fixes σ_{30} and σ_{31}).

We pin down the last free parameter, the point on the bisectrix indicated by $\diamond$ in Fig. 11, and minimize $\mathcal{F}_3(\tau^1) + \mathcal{F}_3(\tau^2) + \mathcal{F}_3(\tau^3) + \mathcal{F}_3(\sigma)$. For $n > 4$, a good approximation to the explicit solution is to place the $\diamond$ at $(.068815616\cos(2\pi/n) + .7098539220)$ times the distance of the point marked $\square$ to the origin. The resulting tessellations are shown in Fig. 12.

We compose the finite tessellation μ, defined by $\sigma \cup \tau$, with a C^1 guide $\mathbf{q}$ of degree 3 that is C^2 at the extraordinary point and sample with $h^{4,4}$. Since $\deg_E(\mathbf{q} \circ \mu) = 3$ and $\deg_E(\partial\mathbf{q}(\mu) \cdot \partial\mu) = 2 + 2$. the derivatives of the G^1 construction $\mathbf{q} \circ \mu$ are reproduced by the sampling and the result is a cap with the following properties (cf. Fig. 13, *right*).

Lemma 5. *The surface of degree* $(4,4)$ *is everywhere curvature continuous except across the edges of* σ *and* τ*, where it is tangent continuous. The surface is curvature continuous at the extraordinary point.*

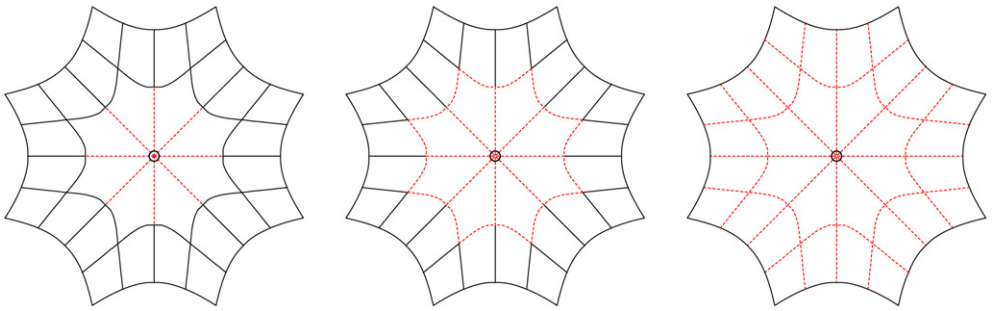

Fig. 13. *Solid* lines indicate curvature continuity, *dashed* (*red*) lines tangent continuity. The surfaces are curvature continuous where *dashed* and *solid* lines meet. In particular, all surface types are curvature continuous at the central point. (*left*) Construction of degree $(6, 6)$. (*middle*) Construction of degree $(5, 5)$. (*right*) Construction of degree $(4, 4)$.

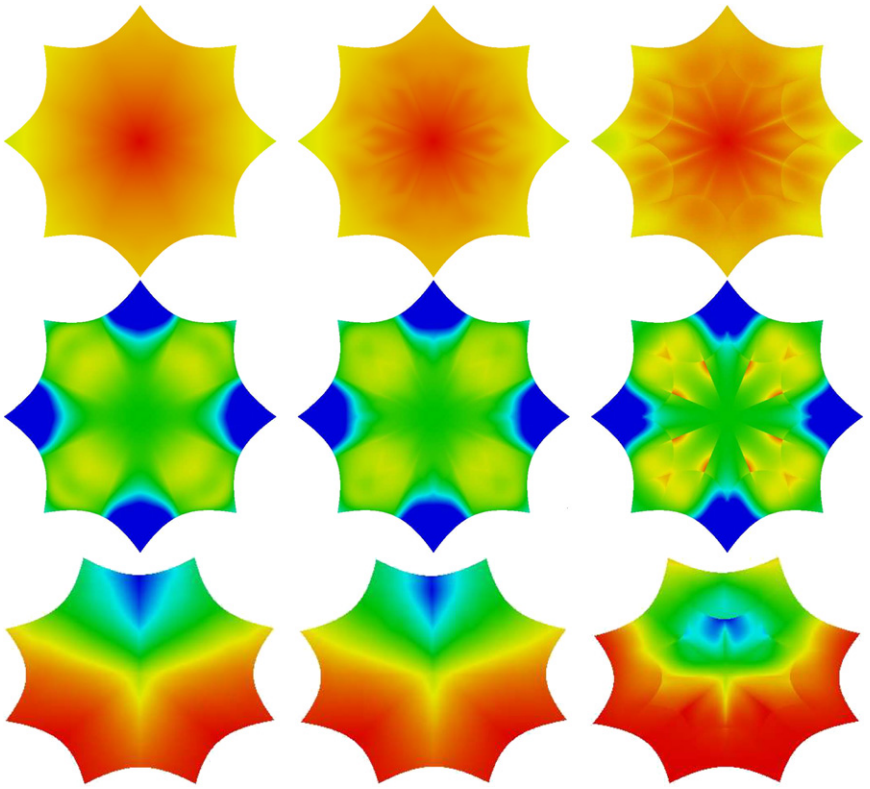

Fig. 14. Gauss curvature of the cap for (from *top* to *bottom*) convex cap, multiple-saddle (same input as in Fig. 8) and single hill in one sector. (from *left* to *right*) degree $(6, 6)$, $(5, 5)$, $(4, 4)$. The curvature images for degree $(8, 8)$ are visually indistinguishable from those of degree $(6, 6)$ and are therefore not additionally displayed.

6. Conclusion

We introduced a new family of surface constructions, whose technical complexity is encapsulated in a finite tessellation μ (of the domain of the guide map). This tessellation is determined once and for all and can be used as a 'black box' submodule since it depends only on the valence and not on the geometric data. The geometric dependence is encapsulated in the guide. The sampling operators and the tessellation link the output surface to the guide surface. The construction can be applied to match second order boundary data across curves up to degree 6. For example, such data are generated by the three recommended initial guided subdivision steps.

To gauge the effect of trading continuity across boundaries for lower degree, we compare the different options on standard examples. Fig. 13 shows the different continuity options. For the standard elliptic test data (Fig. 8, *top*), the overall shape of the family members of degree (k, k), $k \in \{4, 5, 6, 8\}$ is visually indistinguishable. Even Gauss curvature images, when clamped symmetrically about zero and set to the range the boundary data, do not reveal a clear difference in surface quality for different k. Fig. 14 therefore focuses the 'Gauss magnifier' on the central transition and final cap. Only then the Gauss curvature plot reveals, with decreasing k, more of the underlying tessellation of the surface cap. Given the high visual quality even for low k, i.e. low polynomial degree, we expect that each choice of k will find specific applications depending on the need for continuity and constraints on the degree.

Compared to Karčiauskas and Peters (2007c), Karčiauskas and Peters (2007b), the surface quality obtained by all three algorithms does not differ noticeably: the Gauss curvature images are near identical for the standard test cases of convex shape, high-order saddle and flat terrain with a single hill in one sector. The algorithm in Karčiauskas and Peters (2007c, 2007b) achieves exact C^2 continuity using patches of degree at most $(6, 6)$, but the algorithm defined here, in the present paper, has a simpler patch layout.

Acknowledgement

This work was supported by NSF Grants CCF-0430891 and DMI-0400214.

References

Augsdörfer, U.H., Dodgson, N.A., Sabin, M.A., 2006. Tuning subdivision by minimising Gaussian curvature variation near extraordinary vertices. Computer Graphics Forum (Proc. Eurographics) 25 (3), 263–272.

Catmull, E., Clark, J., 1978. Recursively generated B-spline surfaces on arbitrary topological meshes. Computer-Aided Design 10, 350–355.

Cotrina Navau, J., Pla Garcia, N., 2000. Modeling surfaces from planar irregular meshes. Computer Aided Geometric Design 17 (1), 1–15.

Farin, G., 1988. Curves and Surfaces for Computer Aided Geometric Design—A Practical Guide. Academic Press, Boston, MA.

Gregory, J.A., Hahn, J.M., 1989. A C^2 polygonal surface patch. Computer Aided Geometric Design 6 (1), 69–75.

Grimm, C.M., Hughes, J.F., 1995. Modeling surfaces of arbitrary topology using manifolds. Annual Conference Series Computer Graphics 29, 359–368.

Karciauskas, K., Peters, J., 2004. Polynomial C^2 spline surfaces guided by rational multisided patches. In: Jüttler, B. (Ed.), Computational Methods for Algebraic Spline Surfaces. September 29–October 3 2003, Kefermarkt, Austria. Springer, pp. 119–134.

Karčiauskas, K., Peters, J., 2007a. Concentric tessellation maps and curvature continuous guided surfaces. Computer Aided Geometric Design 24 (2), 99–111.

Karčiauskas, K., Peters, J., 2007b. Guided C^2 spline surfaces with V-shaped tessellation. In: Winkler J., Martin R. (Eds.), Mathematics of Surfaces, pp. 233–244.

Karčiauskas, K., Peters, J., 2007c. Parameterization transition for guided C^2 surfaces of low degree. In: Sixth AFA Conference on Curves and Surfaces Avignon, June 29–July 5, 2006, pp. 183–192.

Karciauskas, K., Peters, J., Reif, U., 2004. Shape characterization of subdivision surfaces—case studies. Computer Aided Geometric Design 21 (6), 601–614.

Karčiauskas, K., Myles, A., Peters, J., 2006. A C^2 polar jet subdivision. In: Scheffer, A., Polthier, K. (Eds.), Proceedings of Symposium of Graphics Processing (SGP). June 26–28 2006, Cagliari, Italy. ACM Press, pp. 173–180.

Levin, A., 2006. Modified subdivision surfaces with continuous curvature. In: SIGGRAPH, ACM Transactions on Graphics.

Loop, C., 2004. Second order smoothness over extraordinary vertices. In: Symp. Geom. Processing, pp. 169–178.

Prautzsch, H., Boehm, W., Paluzny, M., 2002. Bézier and B-Spline Techniques. Springer.

Peters, J., 2002a. C^2 free-form surfaces of degree $(3, 5)$. Computer Aided Geometric Design 19 (2), 113–126.

Peters, J., 2002b. Geometric continuity. In: Handbook of Computer Aided Geometric Design. Elsevier, pp. 193–229.

Prautzsch, H., 1997. Freeform splines. Computer Aided Geometric Design 14 (3), 201–206.

Reif, U., 1998. TURBS—topologically unrestricted rational B-splines. Constructive Approximation 14 (1), 57–77.

Ying, L., Zorin, D., 2004. A simple manifold-based construction of surfaces of arbitrary smoothness. ACM TOG 23 (3), 271–275.